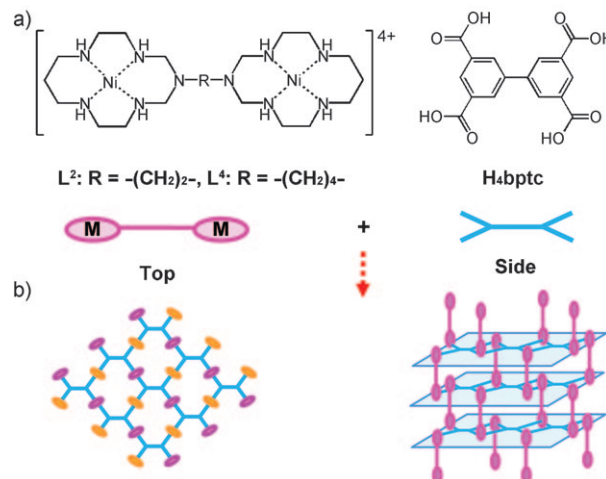


Highly Selective CO₂ Capture in Flexible 3D Coordination Polymer Networks**

Hye-Sun Choi and Myunghyun Paik Suh*

Carbon dioxide capture has been in the center of interests in the scientific community in recent years because of the implications for global warming, and the development of efficient methods for capturing CO₂ from industrial flue gas has become an important issue. It has been revealed that coordination polymer networks (CPNs) with channels or pores can be applied in gas storage,^[1,2] gas separation,^[3] ion exchange,^[4] and selective adsorption of organic or inorganic molecules.^[1e,5-7] It has been reported that large amounts of CO₂ can be adsorbed in some CPNs, for example 20 wt % at 195 K and 1 bar in [[Cu(pyrdc)(bpp)]₂]_n (pyrdc = pyridine-2,3-dicarboxylate, bpp = 1,3-bis(4-pyridyl)propane),^[8a] 16 wt % at 298 K and 50 atm in [Cu(dhbc)₂(4,4'-bpy)] (dhbc = 2,5-dihydroxybenzoate, bpy = bipyridine),^[8b] 114 wt % at 195 K and 1 bar in SNU-6,^[1c] 150 wt % at 298 K and 42 bar in MOF-177,^[9a] and 176 wt % at 303 K and 50 bar in MIL-101c.^[9b] However, the selective capture of CO₂, in particular at ambient temperature and pressure, from industrial emission streams that contain other gases such as N₂, CH₄, and H₂O still remains challenging.^[1c,10,11]

Our approach to selectively capturing CO₂ with porous materials is based on the construction of highly flexible 3D coordination polymer networks whose channels or pores open and close depending on the gas type. Compared to N₂ and H₂, we expected that CO₂ would interact with the host network more efficiently because of its quadrupole moment (-1.4×10^{-39} Cm²) and open up channels that are closed for other gases. Our design strategy for flexible 3D networks is to use 2D grids formed from square-planar Ni^{II} macrocyclic complexes as linear linkers^[3a,6,7a,b,12] and 1,1'-biphenyl-3,3',5,5'-tetracarboxylate (bptc⁴⁻)^[13] as a square organic building block, and then to connect the 2D grids with highly flexible alkyl pillars by utilizing alkyl-bridged Ni^{II} bismacrocyclic complexes such as [Ni₂L²](ClO₄)₄ (**A**) and [Ni₂L⁴](ClO₄)₄·8H₂O (**B**, Scheme 1). We previously prepared a 2D pillared bilayer network that behaves like a sponge from other Ni^{II} bismacrocyclic complexes and 1,3,5-benzenetricarboxylate.^[6] The formation of either 2D or 3D pillared network



Scheme 1. a) Alkyl-bridged Ni^{II} bismacrocyclic complexes and H₄bptc. b) Design strategies for construction of 3D networks. Bismacrocyclic complexes located upward and downward with respect to a 2D plane are indicated by the different colors (pink and orange).

depends on how the bismacrocyclic complex connects 2D planes (Chart S1 in the Supporting Information), which is affected by the pore size of the 2D layer and the steric hindrance between the pillars.

Herein, we report two flexible 3D coordination polymer networks, [(Ni₂L²)(bptc)]·6H₂O·3DEF (**1**, DEF = *N,N*-diethylformamide) and [(Ni₂L⁴)(bptc)]·14H₂O (**2**), which exhibit highly selective CO₂ adsorption over N₂, H₂, and CH₄ gases as well as thermal stability up to 300 °C and air and water stability. The CO₂ adsorption isotherms of **1** and **2** show gate opening and closing phenomena as well as hysteretic desorption, which allow efficient CO₂ capture, storage, and sensing. Compounds **1** and **2** are the first 3D pillared networks assembled from Ni^{II} bismacrocyclic complexes.

The self-assembly of **A** and H₄bptc in DEF/H₂O/TEA (2:3:0.16, v/v; TEA = triethylamine) yielded violet crystals of **1**. The self-assembly of **B** and Na₄bptc in DEF/H₂O (1:4, v/v) afforded **2**. Compounds **1** and **2** are insoluble in water and common organic solvents such as MeOH, EtOH, MeCN, chloroform, acetone, toluene, dimethylformamide, and dimethylsulfoxide.

In the X-ray crystal structure of **1** (Figure 1),^[14] each Ni^{II} macrocyclic unit of **A** is coordinated by two bptc⁴⁻ ligand at the *trans* positions, and each bptc⁴⁻ ligand binds four Ni^{II} ions belonging to four different bismacrocyclic complexes to construct 2D grids extending parallel to the *ab* plane. The 2D grid generates rhombic cavities with effective sizes of 3.32 × 8.14 Å², each of which involves four Ni^{II} macrocyclic units and four bptc⁴⁻ units. The layer is not completely flat, as

[*] H.-S. Choi, Prof. M. P. Suh
 Department of Chemistry, Seoul National University
 Seoul 151-747 (Republic of Korea)
 Fax: (+82) 2-886-8516
 E-mail: mpsuh@snu.ac.kr

[**] This work was supported by a Korea Research Foundation Grant (Basic Research Promotion Fund, KRF-2005-084-C00020), and by the SRC program of MOST/KOSEF through the Center for Intelligent Nano-Bio Materials (grant: R11-2005-008-00000-0).

Supporting information for this article is available on the WWW under <http://dx.doi.org/10.1002/anie.200902836>.

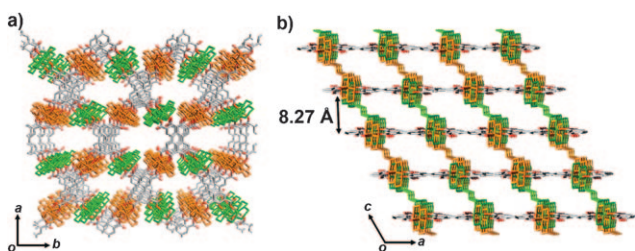


Figure 1. The X-ray crystal structure of **1**. a) A view of the *ab* plane showing the rhombic channels. b) A view of the *ac* plane, showing the tilted ethyl pillars. Color scheme: bptc^{4-} light gray; alternately located Ni^{II} bismacrocylic complexes on the 2D grids brown and green. H atoms are omitted for clarity.

the dihedral angle between the two phenyl rings of bptc^{4-} is $23.24(9)^\circ$. The bismacrocylic complexes are located alternately between two 2D grids; the ethyl bridging group of the bismacrocylic complex acts as a pillar connecting the grids, which gives rise to a pillared-multilayer 3D network. The interlayer distance is 8.72 \AA with the ethyl pillars tilted by 40.5° with respect to the straight line linking the 2D planes. The side channels generated along the $[010]$ and $[100]$ directions have effective aperture sizes of $4.85 \times 12.12 \text{ \AA}^2$ and $1.21 \times 4.37 \text{ \AA}^2$, respectively. The void volume of **1** is 55.8% of the crystal volume, as estimated by PLATON.^[15] The channels are filled with guest solvent molecules, but these could not be located in the X-ray structure (except $6\text{H}_2\text{O}$) because of severe thermal disorder. Therefore, the identity and number of the guest molecules were determined from the IR spectra, elemental analysis, and thermogravimetric analysis (TGA) data (Figure S2 in the Supporting Information). The temperature-dependent powder X-ray diffraction (PXRD) patterns and the TGA data suggest that **1** is thermally stable up to 300°C (Figure S3 in the Supporting Information).

When the guest molecules of **1** were exchanged with various solvents such as MeCN, EtOH, and hexane, the PXRD pattern became different from that of **1**, thus indicating that the host network is flexible enough to change its structure depending on the nature of the guest molecules (Figure S4 in the Supporting Information).^[7a,12a] We exchanged the guest molecules of **1** with MeCN by immersion of **1** in anhydrous MeCN to afford $[(\text{Ni}_2\text{L}^2)(\text{bptc})]\cdot 3\text{MeCN}$ (**1**_{MeCN}) and then removed the MeCN guests by heating **1**_{MeCN} at 100°C under vacuum for 6 h to obtain $[(\text{Ni}_2\text{L}^2)(\text{bptc})]$ (SNU-M10). The PXRD patterns of **1**, a desolvated sample of **1** (**1'**; prepared by drying **1** at 110°C under vacuum for 18 h), **1**_{MeCN}, and SNU-M10 indicated that the network structure changed on exchange and removal of the guest solvent molecules (Figure S5 in the Supporting Information). On immersion of SNU-M10 in MeCN for 6 h, its network structure returned to that of **1**_{MeCN}. Interestingly, even after exposure of SNU-M10 to air for 30 days, the network remained stable as evidenced by PXRD patterns.

The X-ray crystal structure of **2**^[16] is similar to that of **1** (Figure 2). In **2**, the butyl bridging group of bismacrocylic complex **B** acts as a pillar linking the 2D layers that are constructed of Ni^{II} macrocylic species and bptc^{4-} . Contrary

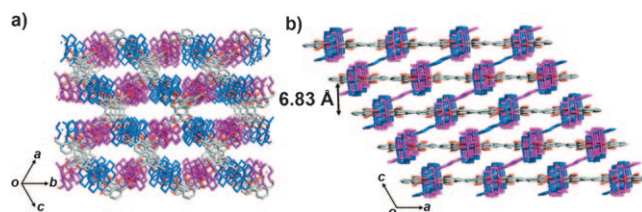


Figure 2. X-ray crystal structure of **2**. a) A view of the (101) plane. b) A view of the *ac* plane, showing the tilted butyl pillars. Color scheme: bptc^{4-} light gray; alternately located Ni^{II} bismacrocylic complexes blue and violet. H atoms are omitted for clarity.

to our expectation, the interlayer distance (6.80 \AA) is significantly shorter than that of **1** (8.72 \AA), because the butyl pillars are much more tilted (68.4°) than the ethyl pillars in **1** (40.5°). Solid **2** generates 1D rhombic channels with an effective aperture size of $1.16 \times 6.29 \text{ \AA}^2$ along the $[101]$ direction, in contrast to **1**, which generates 3D channels. The solvent-accessible free volume of **2** is 35.0% of the total crystal volume, as estimated by PLATON.^[15] The identity and number of the guest water molecules in **2** were determined by the IR spectra, elemental analysis, and TGA data (Figure S8 in the Supporting Information). Temperature-dependent PXRD patterns (Figure S9 in the Supporting Information) and TGA data suggest that **2** is thermally stable up to 300°C .

When **2** was heated at 100°C under vacuum for 12 h, desolvated solid $[(\text{Ni}_2\text{L}^4)(\text{bptc})]$ (SNU-M11) resulted. The PXRD pattern of SNU-M11 was different from that of **2** (Figure S10 in the Supporting Information), thus indicating that the network structure changed on removal of guest water molecules. When SNU-M11 was exposed to air for 5 min, however, the PXRD pattern of **2** was regenerated, indicating that the network structure of **2** was restored by the reintroduction of the guest water molecules. Compound **2** is air- and water-stable; the network was retained even after it had been exposed to air for 30 days or immersed in water for 12 h, as evidenced by the PXRD patterns (Figure S10 in the Supporting Information).

To investigate the gas sorption properties of SNU-M10 and SNU-M11, gas adsorption isotherms were measured for N_2 , H_2 , CH_4 , and CO_2 . SNU-M10 and SNU-M11 hardly adsorb N_2 , H_2 , and CH_4 . As indicated by the X-ray structures, the channel aperture sizes of **1** were big enough, but those of **2** were too small for these gases to enter, and on guest solvent removal, they seem to be much reduced in size by greater tilting of the pillars. However, SNU-M10 and SNU-M11 adsorb large amounts of CO_2 at 195 K and 1 atm (Figure 3 and Figure 4), owing to the quadrupole moment of CO_2 , which induces interaction with the networks to open up the channels.

SNU-M10 adsorbs CO_2 gas at 195 K , exhibiting a type I isotherm (Figure 3). The CO_2 adsorption capacity at 195 K and 1 atm is $24.3 \text{ wt}\%$ ($123.5 \text{ cm}^3 \text{ g}^{-1}$ at STP, 5.5 mmol g^{-1}). The Langmuir surface area estimated from the CO_2 isotherm is $505 \text{ m}^2 \text{ g}^{-1}$, while that estimated from N_2 adsorption at 77 K is $3.24 \text{ m}^2 \text{ g}^{-1}$, which correspond to the internal and external surface areas of SNU-M10, respectively. The pore volume estimated by applying the Dubinin–Radushkevich equation is

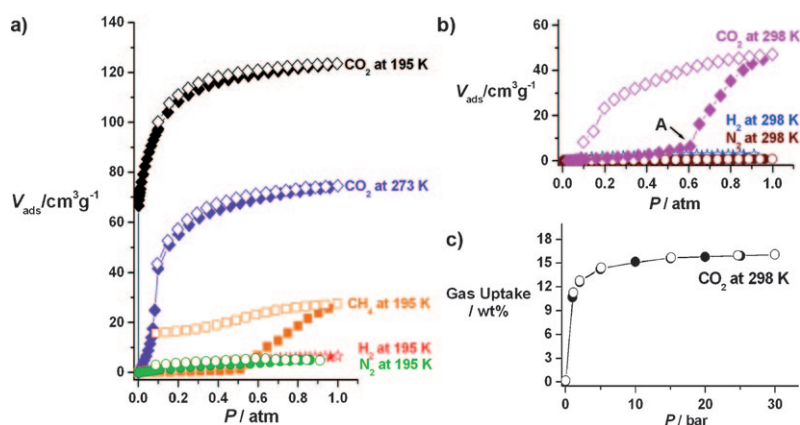


Figure 3. The CO₂ sorption isotherms of SNU-M10. a) Measured at 195 (black) and 273 K (purple) up to 1 atm compared to the sorption isotherms of CH₄ (orange), N₂ (green), and H₂ (red). b) Measured at 298 K (pink) up to 1 atm compared to the sorption isotherms of N₂ (brown) and H₂ (blue). c) Excess CO₂ sorption measured at 298 K up to 30 bar. Filled shapes: adsorption. Open shapes: desorption.

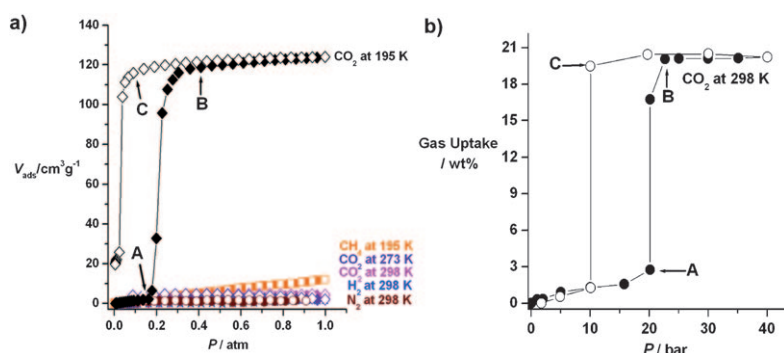


Figure 4. The CO₂ sorption isotherms of SNU-M11. a) Measured at 195 (black), 273 (purple), and 298 K (pink) up to 1 atm compared to the sorption isotherms of CH₄ (orange), N₂ (brown), and H₂ (blue). b) Excess CO₂ sorption measured at 298 K up to 40 bar. Filled shapes: adsorption. Open shapes: desorption. See text for details of points A, B, and C.

0.20 cm³ g⁻¹. At 273 K, the CO₂ adsorption isotherm shows an S-shaped curve, indicating 14.6 wt% (74.6 cm³ g⁻¹ at STP, 3.3 mmol g⁻¹) of CO₂ uptake at 1 atm. At 298 K and 1 atm, SNU-M10 adsorbs almost no CO₂ until 0.61 atm (point A; the gate-opening pressure, P_{go}), at which it abruptly starts to adsorb CO₂ and then reaches 9.2 wt% (47.2 cm³ g⁻¹ at STP, 2.1 mmol g⁻¹) CO₂ uptake at 1 atm. The desorption isotherm at 298 K shows a large hysteresis; the adsorbed gas is gradually released in the regime of 1.0–0.2 atm and sharply desorbed at the lower pressures. The high-pressure CO₂ sorption isotherm indicates that SNU-M10 exhibits excess CO₂ adsorption capacity of 15.2 wt% at 298 K and 10 bar.

SNU-M11 also adsorbs CO₂ gas at 195 K, but not at 273 and 298 K (Figure 4a). At 195 K, it hardly adsorbs CO₂ gas up to 0.18 atm (point A, P_{go}), where it suddenly starts to adsorb the gas and then reaches a plateau at 0.41 atm (point B). The CO₂ adsorption capacity at 1 atm is 24.4 wt% (124.0 cm³ g⁻¹ at STP, 5.54 mmol g⁻¹). The desorption isotherm does not retrace the adsorption curve, but exhibits a large hysteresis:

SNU-M11 maintains the amount of adsorbed CO₂ until the pressure is lowered to 0.039 atm (point C, gate-closing pressure, P_{gc}), at which CO₂ is abruptly desorbed. Although SNU-M11 does not adsorb CO₂ gas at 273 and 298 K up to 1 atm, it adsorbs the gas at higher pressures (Figure 4b). At 298 K, it starts adsorbing CO₂ at 20.0 bar (point A, P_{go}) and reaches 20.6 wt% CO₂ uptake at 23 bar (point B), which is more than the 15.2 wt% for SNU-M10. The desorption isotherm exhibits a large hysteresis, and the adsorbed CO₂ cannot be released until 10.0 bar (point C, P_{gc}).

For both SNU-M10 and SNU-M11, the CO₂ adsorption isotherms exhibit gate-opening phenomena as well as large hysteretic desorption, which is attributed to the flexibility of the networks. The gate-opening pressure increases as the temperature increases, similarly to the adsorptions of H₂, Ar, N₂, and O₂ in other flexible networks.^[17] At the gate-opening pressure, CO₂ molecules, which have a quadrupole moment (-1.4×10^{-39} Cm²),^[11,18] induce structural transformation of the network from the closed phase to the open phase. The fact that SNU-M10 shows lower gate-opening pressure than SNU-M11 at the same temperature suggests that the ethyl pillars in SNU-M10 are more flexible than the butyl pillars in SNU-M11. The gate-opening energy (ΔH_{go}) of SNU-M10 for CO₂ uptake, which is calculated using the Clausius–Clapeyron equation, is 27.6 kJ mol⁻¹ (Figure S14 in the Supporting Information).

The synchrotron PXRD patterns of SNU-M10 measured under vacuum indicate that the network structure is independent of temperature at 195, 273, and 298 K (Figure S15 in the Supporting Information). However, at 1 atm CO₂ and 298 K, several peaks of the PXRD pattern shift to the lower angle region compared to those measured under vacuum, indicating the expansion of the network on CO₂ adsorption (Figure 5).

Although the CO₂ sorption capacities at 298 K for SNU-M10 (9.3 wt% at 1 atm and 15 wt% at 10 bar) and SNU-M11 (21 wt% at 30 bar) are lower than the highest values reported so far for MOFs (149 wt% in MOF-177 at 42 bar),^[9a] the present coordination polymer networks show extraordinary high selectivity for adsorption of CO₂ over N₂, H₂, and CH₄ at room temperature. The CO₂/N₂ selectivity of SNU-M10 at 298 K is 24:1 (v/v) at 0.61 atm and 98:1 (v/v) at 1.0 atm. For the application of a network as a CO₂ capture material, the selectivity for adsorption of CO₂ over N₂ is highly important.

The selective and reversible capture of CO₂ in SNU-M10 at 298 K was also verified by the gas cycling experiment on a thermogravimetric apparatus using a flow of 15% (v/v) CO₂ in N₂, which approximately mimics flue gas, followed by a flow of pure N₂ gas (Figure 6). A reversible change of 0.77 wt% was observed over the cycles, and the material was regenerated by the N₂ gas flow. This result suggests that SNU-

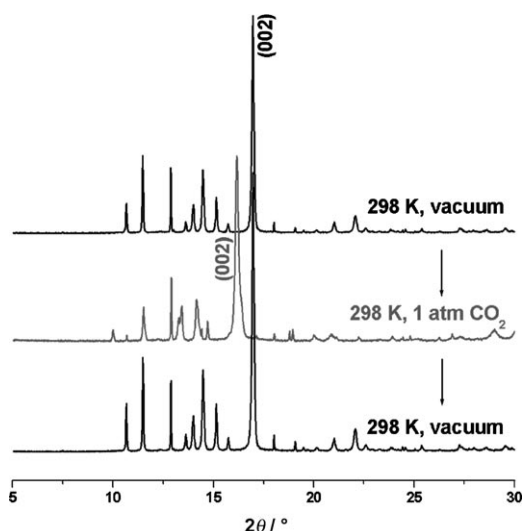


Figure 5. In-situ synchrotron powder X-ray diffraction patterns of SNU-M10 measured under vacuum, at 1 atm of CO₂ pressure, and again under vacuum (CuK α , λ = 1.54178 Å). The peaks at 2θ = 16.96° under vacuum and 16.15° under 1 atm CO₂ correspond to the (002) plane.

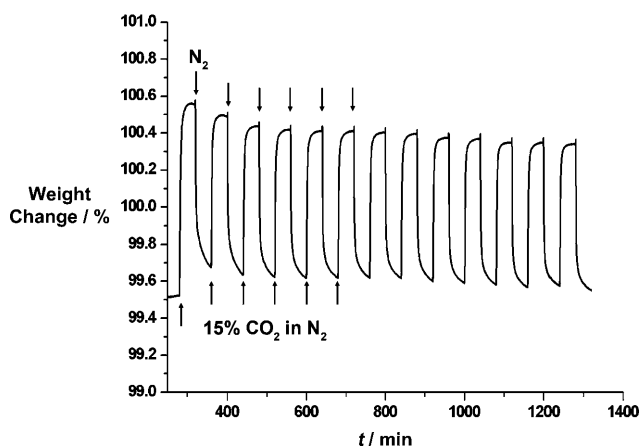


Figure 6. Gas cycling data measured on a thermogravimetric instrument for SNU-M10 at 298 K, using a stream of 15% (v/v) CO₂ in N₂ followed by pure N₂.

M10 is a very good candidate material that can be applied in a pressure swing type CO₂ sequestration process.

In conclusion, we have prepared highly flexible 3D pillared coordination networks, for the first time by using Ni^{II} bismacroyclic complexes. The networks can open and close their channels depending on the gas type, temperature, and pressure. The X-ray crystal structures indicate that alkyl pillars connecting the 2D square grids are significantly tilted (40.5° for the ethyl pillars in **1** and 68.4° for the butyl pillars in **2**). The desolvated solids obtained from **1** and **2**, SNU-M10 and SNU-M11, exhibit highly selective adsorption of CO₂ over N₂, H₂, and CH₄ gases along with thermal stability to 300°C and air and water stability. Typically, the CO₂/N₂ selectivity in SNU-M10 is 98:1 (v/v) at 298 K and 1 atm. The CO₂ adsorption isotherms of both networks show gate-opening phenomena and large hysteric desorption. The gate-opening pressure for SNU-M10 is lower than that for

SNU-M11 at the same temperature, indicating the higher flexibility of the ethyl pillars than the butyl pillars. The gate-opening energy of SNU-M10 for CO₂ uptake is 27.6 kJ mol⁻¹. Selective and reversible CO₂ adsorption has been also verified by gas cycling experiments. The present 3D coordination networks incorporating flexible pillars can be applied in the selective capture, storage, and sensing of CO₂ gas as well as in the separation of the CO₂/H₂ mixture resulting from the water gas shift reaction and might function as selective membranes in other applications.

Received: May 27, 2009

Revised: June 30, 2009

Published online: August 19, 2009

Keywords: adsorption · carbon dioxide capture · macrocyclic complexes · nickel · organic–inorganic hybrid composites

- [1] a) Y. E. Cheon, M. P. Suh, *Angew. Chem.* **2009**, *121*, 2943–2947; *Angew. Chem. Int. Ed.* **2009**, *48*, 2899–2903; b) Y.-G. Lee, H. R. Moon, Y. E. Cheon, M. P. Suh, *Angew. Chem.* **2008**, *120*, 7855–7859; *Angew. Chem. Int. Ed.* **2008**, *47*, 7741–7745; c) H. J. Park, M. P. Suh, *Chem. Eur. J.* **2008**, *14*, 8812–8821; d) M. P. Suh, Y. E. Cheon, E. Y. Lee, *Chem. Eur. J.* **2007**, *13*, 4208–4215; e) E. Y. Lee, S. Y. Jang, M. P. Suh, *J. Am. Chem. Soc.* **2005**, *127*, 6374–6381; f) E. Y. Lee, M. P. Suh, *Angew. Chem.* **2004**, *116*, 2858–2861; *Angew. Chem. Int. Ed.* **2004**, *43*, 2798–2801.
- [2] a) S. S. Kaye, A. Dailly, O. M. Yaghi, J. R. Long, *J. Am. Chem. Soc.* **2007**, *129*, 14176–14177; b) S. Ma, D. Sun, J. M. Simmons, C. D. Collier, D. Yuan, H.-C. Zhou, *J. Am. Chem. Soc.* **2008**, *130*, 1012–1016; c) L. J. Murray, M. Dincă, J. R. Long, *Chem. Soc. Rev.* **2009**, *38*, 1294–1314; d) D. Britt, D. Tranchemontagne, O. M. Yaghi, *Proc. Natl. Acad. Sci. USA* **2008**, *105*, 11623–11627.
- [3] a) Y. E. Cheon, M. P. Suh, *Chem. Eur. J.* **2008**, *14*, 3961–3967; b) Y. E. Cheon, M. P. Suh, *Chem. Commun.* **2009**, 2296–2298; c) H. R. Moon, N. Kobayashi, M. P. Suh, *Inorg. Chem.* **2006**, *45*, 8672–8676; d) R. Banerjee, H. Furukawa, D. Britt, C. Knobler, M. O’Keeffe, O. M. Yaghi, *J. Am. Chem. Soc.* **2009**, *131*, 3875–3877; e) S. Ma, X.-S. Wang, D. Yuan, H.-C. Zhou, *Angew. Chem.* **2008**, *120*, 4198–4201; *Angew. Chem. Int. Ed.* **2008**, *47*, 4130–4133; f) J.-R. Li, Y. Tao, Q. Yu, Z.-H. Bu, H. Sakamoto, S. Kitagawa, *Chem. Eur. J.* **2008**, *14*, 2771–2776.
- [4] a) K. S. Min, M. P. Suh, *J. Am. Chem. Soc.* **2000**, *122*, 6834–6840; b) H. J. Choi, M. P. Suh, *Inorg. Chem.* **2003**, *42*, 1151–1157; c) M. J. Manos, R. Iyer, G. E. Quarez, J. H. Liao, M. G. Kanatzidis, *Angew. Chem.* **2005**, *117*, 3618–3621; *Angew. Chem. Int. Ed.* **2005**, *44*, 3552–3555; d) P. N. Trikalitis, K. K. Rangan, T. Bakas, M. G. Kanatzidis, *J. Am. Chem. Soc.* **2002**, *124*, 12255–12260; e) M. Dincă, J. R. Long, *J. Am. Chem. Soc.* **2007**, *129*, 11172–11176.
- [5] H. J. Kim, M. P. Suh, *Inorg. Chem.* **2005**, *44*, 810–812.
- [6] a) M. P. Suh, J. W. Ko, H. J. Choi, *J. Am. Chem. Soc.* **2002**, *124*, 10976–10977; b) H. J. Choi, M. P. Suh, *J. Am. Chem. Soc.* **2004**, *126*, 15844–15851.
- [7] a) J. W. Ko, K. S. Min, M. P. Suh, *Inorg. Chem.* **2002**, *41*, 2151–2157; b) K. S. Min, M. P. Suh, *Chem. Eur. J.* **2001**, *7*, 303–313; c) B. Chen, J. Liang, J. Yang, D. S. Contreras, Y. L. Clancy, E. B. Lobkovsky, O. M. Yaghi, S. Dai, *Angew. Chem.* **2006**, *118*, 1418–1421; *Angew. Chem. Int. Ed.* **2006**, *45*, 1390–1393; d) J. Y. Lee, D. H. Olson, L. Pan, T. J. Ernge, J. Li, *Adv. Funct. Mater.* **2007**, *17*, 1255–1262.

- [8] a) T. K. Maji, G. Mostafa, R. Matsuda, S. Kitagawa, *J. Am. Chem. Soc.* **2005**, *127*, 17152–17153; b) R. Kitaura, K. Seki, G. Akiyama, S. Kitagawa, *Angew. Chem.* **2003**, *115*, 444–447; *Angew. Chem. Int. Ed.* **2003**, *42*, 428–431.
- [9] a) A. R. Millward, O. M. Yaghi, *J. Am. Chem. Soc.* **2005**, *127*, 17998–17999; b) P. L. Llewellyn, S. Bourrelly, C. Serre, A. Vimont, M. Daturi, L. Hamon, G. D. Weireld, J. Chang, D. Hong, Y. K. Hwang, S. H. Jung, G. Férey, *Langmuir* **2008**, *24*, 7245–7250.
- [10] a) B. Wang, A. P. Côté, H. Furukawa, M. O’Keefe, O. M. Yaghi, *Nature* **2008**, *453*, 207–212; b) R. Banerjee, A. Phan, B. Wang, C. Knobler, H. Furukawa, M. O’Keefe, O. M. Yaghi, *Science* **2008**, *319*, 939–941; c) P. K. Thallapally, J. Tian, M. R. Kishan, C. A. Fernandez, S. J. Dalgarno, P. B. McGrail, J. E. Warren, J. L. Atwood, *J. Am. Chem. Soc.* **2008**, *130*, 16842–16843.
- [11] a) P. L. Llewellyn, S. Bourrelly, C. Serre, Y. Filinchuk, G. Férey, *Angew. Chem.* **2006**, *118*, 7915–7918; *Angew. Chem. Int. Ed.* **2006**, *45*, 7751–7754; b) L. Bastin, P. S. Bárcia, E. J. Hurtado, J. C. Silva, A. E. Rodrigues, B. Chen, *J. Phys. Chem. C* **2008**, *112*, 1575–1581; c) S. Couck, J. M. Denayer, G. V. Baron, T. Remy, J. Gascon, F. Kapteijin, *J. Am. Chem. Soc.* **2009**, *131*, 6326–6327.
- [12] a) H. J. Choi, M. P. Suh, *J. Am. Chem. Soc.* **1998**, *120*, 10622–10628; b) M. P. Suh, H. R. Moon, E. Y. Lee, S. Y. Jang, *J. Am. Chem. Soc.* **2006**, *128*, 4710–4718; c) M. P. Suh, Y. E. Cheon, E. Y. Lee, *Coord. Chem. Rev.* **2008**, *252*, 1007–1026; d) M. P. Suh, H. R. Moon, *Adv. Inorg. Chem.* **2007**, *59*, 39–79.
- [13] B. Chen, N. W. Ockwig, A. R. Millward, D. S. Contreras, O. M. Yaghi, *Angew. Chem.* **2005**, *117*, 4823–4827; *Angew. Chem. Int. Ed.* **2005**, *44*, 4745–4749.
- [14] Crystal data for **1**: Ni₂C₃₆H₅₄N₁₀O₈, $M_r = 872.31$, monoclinic, space group *C2/c*, $a = 25.2087(5)$, $b = 16.2843(3)$, $c = 19.9379(4)$ Å, $\beta = 119.319(1)^\circ$, $V = 7136.2(2)$ Å³, $Z = 4$, $\rho_{\text{calcd}} = 0.812$ g cm⁻³ without guests, $\mu = 0.563$ mm⁻¹, $\lambda = 0.71073$ Å, $T = 298(2)$ K, $2\theta = 54.98^\circ$, 253 parameters, $R_1 = 0.0549$ ($I > 2\sigma(I)$, 8140 reflections), $wR_2 = 0.1709$ (all data, 14081 reflections), GOF = 0.947.
- [15] A. L. Spek, *PLATON A Multipurpose Crystallographic Tool*, Utrecht University, Utrecht, **2007**.
- [16] Crystal data for **2**: Ni₂C₃₈H₅₈N₁₀O₈, $M_r = 900.36$, monoclinic, space group *C2/c*, $a = 25.1189(12)$, $b = 16.3750(9)$, $c = 16.6616(10)$ Å, $\beta = 125.254(2)^\circ$, $V = 5596.4(5)$ Å³, $Z = 4$, $\rho_{\text{calcd}} = 1.069$ g cm⁻³ without guests, $\mu = 0.720$ mm⁻¹, $\lambda = 0.71073$ Å, $T = 298(2)$ K, $2\theta = 55.04^\circ$, 263 parameters, $R_1 = 0.1210$ ($I > 2\sigma(I)$, 5769 reflections), $wR_2 = 0.3430$ (all data, 10259 reflections), GOF = 0.904. CCDC 727773 (**1**) and 727774 (**2**) contain the supplementary crystallographic data for this paper. These data can be obtained free of charge from The Cambridge Crystallographic Data Centre via www.ccdc.cam.ac.uk/data_request/cif.
- [17] a) D. Tanaka, K. Nakagawa, M. Higuchi, S. Horike, Y. Kubota, T. C. Kabayashi, M. Takata, S. Kitagawa, *Angew. Chem.* **2008**, *120*, 3978–3982; *Angew. Chem. Int. Ed.* **2008**, *47*, 3914–3918; b) H. J. Choi, M. Dincă, J. R. Long, *J. Am. Chem. Soc.* **2008**, *130*, 7848–7850.
- [18] Y.-S. Bae, O. K. Farha, A. M. Spokoyny, C. A. Mirkin, J. T. Hupp, R. Q. Snurr, *Chem. Commun.* **2008**, 4135–4137.